

# Structural, electrical and electrochemical properties of co-precipitated $\text{SrFeO}_{3-\delta}$

C.O. Augustin\*, L. John Berchmans, R. Kalai Selvan

*Central Electrochemical Research Institute, Karaikudi-630 006, India*

Received 17 June 2003; accepted 16 September 2003

## Abstract

The non-stoichiometric perovskite-type oxide  $\text{SrFeO}_{3-\delta}$  was prepared by Co-precipitation method using metal nitrate salts as cation precursors and NaOH solution as the precipitating agent. From the thermogravimetric analysis, the strontium orthoferrite phase formation was found to be complete at 550 °C. The XRD spectra showed the synthesized compound to be of orthorhombic structure. The FTIR spectra confirm the characteristic peaks of  $\text{SrFeO}_{3-\delta}$  stretching and bending vibrations. The submicron size of the synthesized compound was showed by scanning electron microscope. The physical properties such as density, porosity and hardness were also carried out. The DC electrical conductivity measurements gave the maximum value of  $84 \text{ S cm}^{-1}$  for the 1000 °C sintered sample. The electrochemical behavior of the 800 and 1000 °C sintered  $\text{SrFeO}_{3-\delta}$  electrode was performed in alkaline KOH solution by potentiostatic polarization and electrochemical impedance spectroscopy.

© 2003 Elsevier B.V. All rights reserved.

*Keywords:* Co-precipitation; Thermal analysis; X-ray diffraction; Infrared spectroscopy; DC conductivity

## 1. Introduction

The mixed oxide based composites, generally of spinel and perovskite structures are extensively studied for their virtual properties. In particular, the perovskite materials occupy a prominent place in the materials science world because of its very favourable characteristics such as structural, ionic as well as electronic conductivity, high electrocatalytic activity and high thermodynamic stability. They are immensely used as electrode materials for solid oxide fuel cells, batteries, oxygen-permeable membranes, pressure-driven oxygen generators and water electrolytic systems [1–3]. This work envisages the use of perovskite-type materials as anodes for extractive metallurgical processes. The increasing awareness of energy, environment and economy demands the replacement of conventionally used carbon anodes due to the evolution of obnoxious fumes  $\text{CO}_2$ , CO,  $\text{CF}_6$ , etc. [4]. The  $\text{SrFeO}_{3-\delta}$  is identified to thrive as a suitable electrode for  $\text{O}_2$  evolution in alkaline and molten salt systems due to its high electronic and ionic

conductivity, thermal stability and low chemical leachability. Of the known synthetic methods, co-precipitation is preferred because of its advantages over the other methods such as atomic/molecular level homogeneous mixing of constituent metal ions, better reactivity at lower reaction temperatures, high purity, and good control of stoichiometry and high sinterability [5].

This paper deals with the structural, electrical and electrochemical properties of  $\text{SrFeO}_{3-\delta}$  prepared by Co-precipitation method. The structural and morphological characteristics were studied by using XRD, FTIR and SEM, and electrical properties by using a modified four-probe technique and electrochemical studies by using potentiostatic polarization and electrochemical impedance spectroscopy.

## 2. Experimental

The non-stoichiometric  $\text{SrFeO}_{3-\delta}$  was synthesized by nonconventional co-precipitation method. The stoichiometric quantities of  $\text{Sr}(\text{NO}_3)_2$  and  $\text{Fe}(\text{NO}_3)_3$  salts were dissolved in triple distilled water. The mixed nitrate solution was added slowly into the alkaline NaOH

\* Corresponding author. Fax: +91-4565-227779, +91-4565-227713.

E-mail address: [caugustin@rediffmail.com](mailto:caugustin@rediffmail.com) (C.O. Augustin).

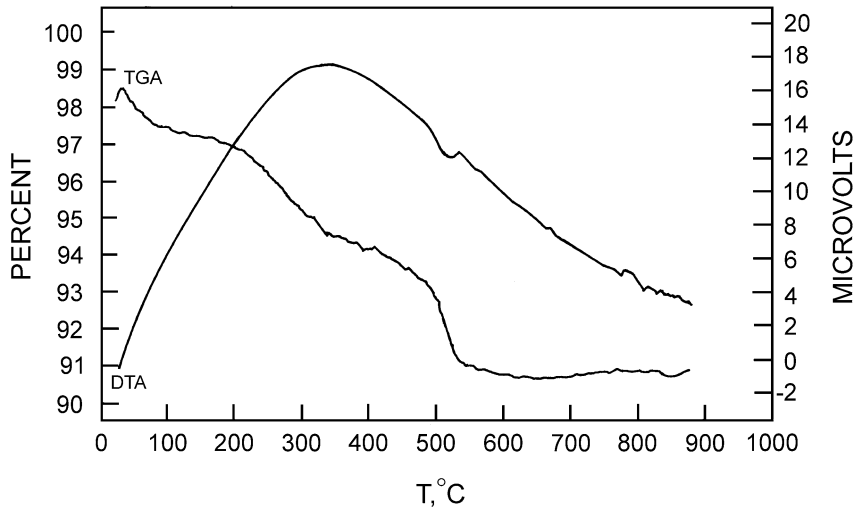


Fig. 1. TG/DTA curve of as-synthesized Co-precipitated  $\text{SrFeO}_{3-\delta}$ .

solution with constant stirring. The precipitate formed at room temperature was filtered using G4 sintered crucible and washed using distilled water followed by ethanol for several times [6].

The as prepared powders were pressed into pellets by applying a pressure  $3.5 \text{ tons/cm}^2$  using hydraulic press. The compacted pellets were sintered at different temperatures, namely at  $600^\circ\text{C}$ ,  $800^\circ\text{C}$  and a final temperature of  $1000^\circ\text{C}$ . The phase formation and structural features

of the synthesized samples were characterized by X-ray powder diffraction (XRD) patterns using  $\text{CuK}\alpha$  ( $\lambda = 1.541 \text{ \AA}$ ) radiation with  $2\theta$  value ranges from  $10^\circ$  to  $80^\circ$  in JEOL 8030 X-ray diffractometer. The FT-IR spectra of

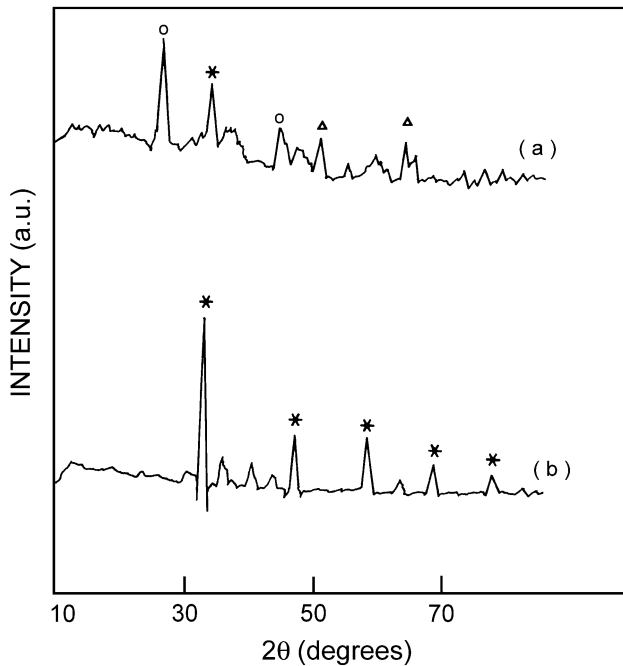


Fig. 2. XRD pattern of (a) as synthesized and (b)  $1000^\circ\text{C}$  sintered  $\text{SrFeO}_{3-\delta}$  sample (\*)  $\text{SrFeO}_{3-\delta}$ , (O)  $\text{SrO}$ , and ( $\blacktriangle$ )  $\text{Fe}_2\text{O}_3$ .

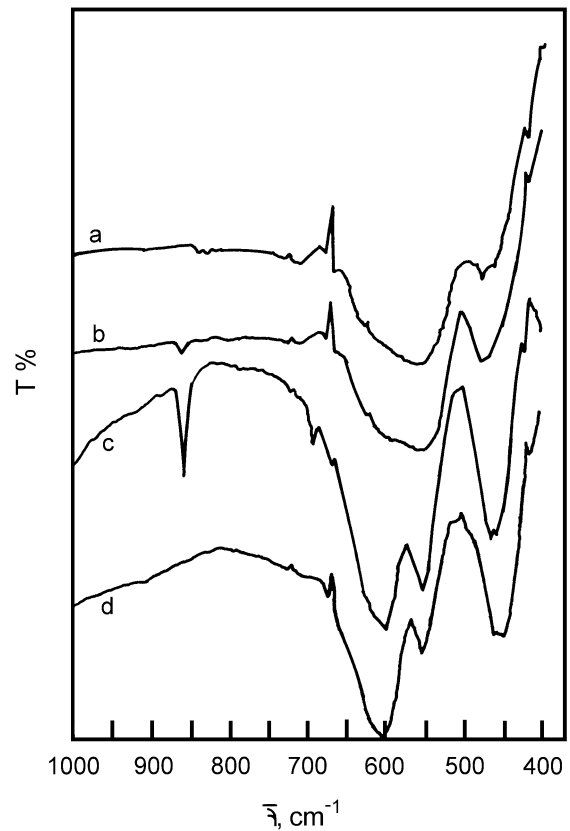


Fig. 3. FTIR spectra of (a) green, (b) sintered at  $600^\circ\text{C}$ , (c)  $800^\circ\text{C}$  and (d)  $1000^\circ\text{C}$   $\text{SrFeO}_{3-\delta}$  samples.

the samples were recorded as KBr discs in the range 400–1000  $\text{cm}^{-1}$  by using FTIR-Perkin Elmer, UK Paragon-500. Scanning electron microscope (SEM) JEOL (JSM-3.5 CF) Japan-made model was employed for the morphological studies. Differential thermal analysis and thermogravimetry (TGA/DTA) of green samples were carried out using Perkin-Elmer TG-7 thermal analyzer and DTA-700. Samples were heated from room temperature to 900  $^{\circ}\text{C}$  at a heating rate of 10  $^{\circ}\text{C min}^{-1}$  under normal atmosphere. The density was calculated by weight and volume method, porosity was measured by liquid absorption technique and hardness was obtained by Vickers hardness tester. The DC electrical conductivity was measured as a function of temperature of the sintered specimens using the modified four-probe method from room temperature to 1000  $^{\circ}\text{C}$  described elsewhere [7]. Electrochemical polarization studies were performed in 1 M KOH solutions using Volta lab-PGA201 Potentiostat/Galvanostat. Impedance measurements were studied using PARC Electrochemical Impedance System. A conven-

al three-electrode system was used for the electrochemical measurements. A 'Pt' foil was used as a counter electrode; a saturated Hg/HgO/1 M KOH electrode was used as the reference electrode. The sintered 1.0 cm diameter with 0.5 cm thickness bulk material was used as the working electrode. The  $C_{dl}$  of the  $\text{SrFeO}_{3-\delta}$  electrode was estimated by extrapolating the linear capacitance region to the  $\log |Z|$  axis at  $\omega=1$  or  $f=0.16$  Hz as described elsewhere [8].

### 3. Results and discussion

#### 3.1. Synthesis

Using co-precipitation method, the  $\text{SrFeO}_{3-\delta}$  fine crystallites were obtained from aqueous solid solutions of  $\text{Sr}(\text{NO}_3)_2$  and  $\text{Fe}(\text{NO}_3)_3$ . In this method, first the nucleation occurs which is followed by subsequent growth of fine crystallites. In the presence of alkaline NaOH medium, the

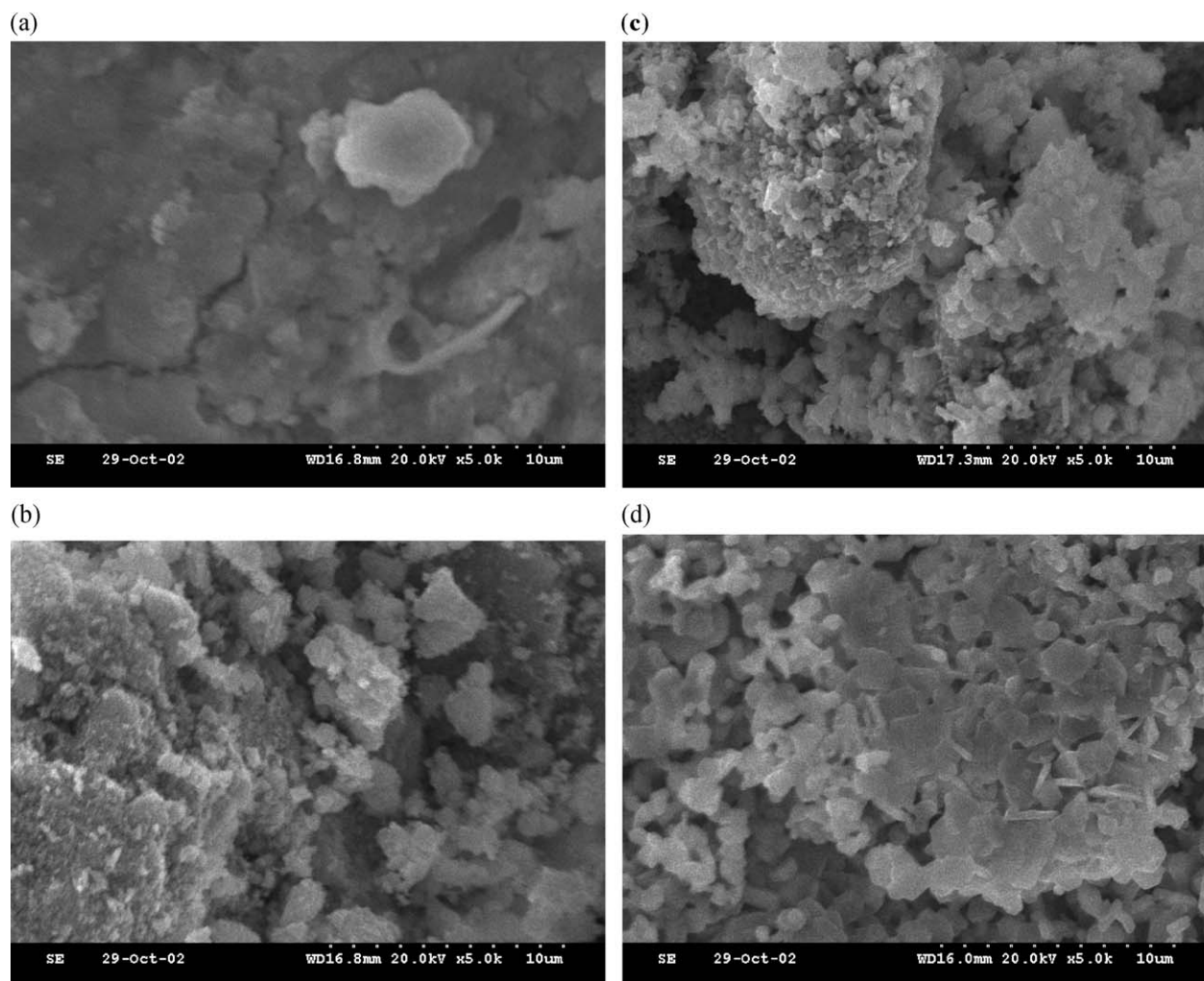
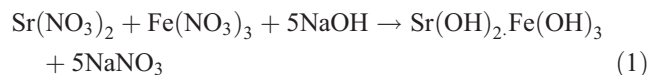


Fig. 4. SEM micrographs of (a) green, (b) sintered at 600  $^{\circ}\text{C}$ , (c) 800  $^{\circ}\text{C}$  and (d) 1000  $^{\circ}\text{C}$   $\text{SrFeO}_{3-\delta}$  samples.

metal cations are dispersed and then form metal hydroxides in the form of colloidal particles.



The above precursor is subjected to heating which transform metal hydroxides to intended ferrites.

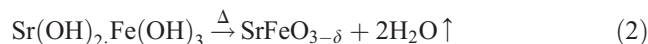


Fig. 1 shows the TG/DTA curves of as prepared  $\text{SrFeO}_{3-\delta}$  samples with a heating rate of  $10^\circ\text{C}/\text{min}$  in static air. From the TGA curve, four distinct weight loss steps are observed. The first weight loss from room temperature to  $232^\circ\text{C}$  may be attributed to the loss of absorbed water or other impurities. The second weight loss from  $232$  to  $340^\circ\text{C}$  was mainly due to the nitrate decomposition and third one  $340$ – $490^\circ\text{C}$  was evaporation of excessive  $\text{NaNO}_3$  in the  $\text{SrFeO}_{3-\delta}$  sample. The final weight loss from  $490$  to  $550^\circ\text{C}$ , a sharp decrease is observed due to the compound formation. After  $550^\circ\text{C}$  no weight loss is observed, which infers the formation of  $\text{SrFeO}_{3-\delta}$  well within the lower processing temperature of  $550^\circ\text{C}$ . From the DTA curve, there is no significant exo/endermic peaks are observed. A broad peak observed at  $346^\circ\text{C}$  may be due to the decomposition of nitrate salts, and a small exothermic peak is observed around  $540^\circ\text{C}$  due to the compound formation.

### 3.2. Structural properties

The powder X-ray powder diffraction patterns of the co-precipitated green and  $1000^\circ\text{C}$  sintered samples are shown in Fig. 2a and b. From Fig. 2a, the materials are found to show the corresponding peaks of  $\text{SrFeO}_{3-\delta}$ ,  $\text{SrO}$  and  $\text{Fe}_2\text{O}_3$ . The well-defined, sharp peak with complete compound formation is observed only in  $1000^\circ\text{C}$  sintered sample (Fig. 2b). The XRD pattern of the  $1000^\circ\text{C}$  sintered  $\text{SrFeO}_{3-\delta}$  sample shows orthorhombic structure near to brownmillerite structure and the lattice parameters of  $a=5.512 \text{ \AA}$ ,  $b=15.6 \text{ \AA}$  and  $c=5.53 \text{ \AA}$ . At room temperature, the materials show tetragonal structure with lattice parameters  $a=10.12 \text{ \AA}$  and  $c=7.624 \text{ \AA}$ . The above lattice parameters are well agreed with the earlier reported values [9,10].

The FTIR spectra of as prepared and sintered  $\text{SrFeO}_{3-\delta}$  samples are shown in Fig. 3 in the frequency range of  $400$ – $1000 \text{ cm}^{-1}$ . According to Last [11], the perovskite samples show two main absorption bands in the above said region.

Table 1  
Physical properties

Sample	Density ( $\text{g}/\text{cm}^3$ )	Porosity (%)	Hardness (VPN)
Green	3.3	14	–
$600^\circ\text{C}$	3.1	27	130
$800^\circ\text{C}$	3.0	34	133
$1000^\circ\text{C}$	2.8	37	150

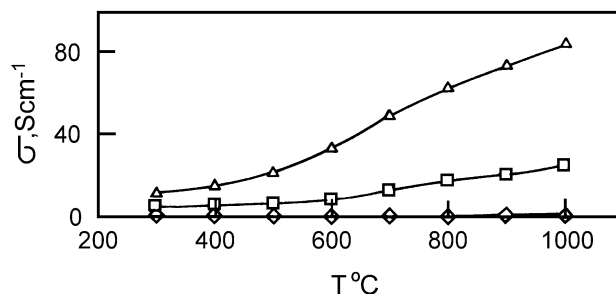


Fig. 5. Electrical conductivity vs. temperature ( $-\diamond-$ ) sintered at  $600^\circ\text{C}$ , ( $-\square-$ )  $800^\circ\text{C}$  and ( $-\triangle-$ )  $1000^\circ\text{C}$ .

The asymmetric higher frequency band  $\gamma_1$  extends from  $800$  to  $475 \text{ cm}^{-1}$  with a center of  $540 \text{ cm}^{-1}$  due to the stretching vibration of metal ions. The lower frequency band  $\gamma_2$  extends from  $475$  to  $300 \text{ cm}^{-1}$  with a center at  $400 \text{ cm}^{-1}$  due to the bending vibration. The higher frequency band  $\gamma_1$  has a value of  $546.29 \text{ cm}^{-1}$  for green sample,  $554.06 \text{ cm}^{-1}$  for  $600^\circ\text{C}$  sintered sample,  $602 \text{ cm}^{-1}$  for  $800^\circ\text{C}$  sintered sample, and  $602 \text{ cm}^{-1}$  for  $1000^\circ\text{C}$  for sintered sample. It can be seen that an increase in sintering temperature enhances the compound formation, which is confirmed by the higher frequency band shifted from lower value to higher value. The lower frequency bands  $\gamma_2$  are  $475.2$ ,  $472$ ,  $466$  and  $449 \text{ cm}^{-1}$  for green, sintered  $600$ ,  $800$  and  $1000^\circ\text{C}$  samples, respectively. The single phase formed at  $1000^\circ\text{C}$  shows strong absorption bands at  $553 \text{ cm}^{-1}$  which corresponds to the stretching vibration of  $\text{Fe-O}$  bonds [12]. The increasing sintering temperature causes the higher frequency band to split into two absorption bands due to the  $\text{SrFeO}_{3-\delta}$  compound formation. This defect structure arises due to the production of oxygen vacancies by  $\text{Sr}^{2+}$  ions [13].

Fig. 4 shows the SEM microphotographs of synthesized  $\text{SrFeO}_{3-\delta}$  green and sintered  $600$ ,  $800$  and  $1000^\circ\text{C}$ . It is evident that as sintering temperature increases, the materials show porous nature with submicron size crystallite formation but in irregular shapes. The grain-to-grain connectivity in the materials is noticed to increase with increase in sintering temperature, which in turn enhances the electrical conductivity [14].

### 3.3. Physical properties

The physical properties of the green and  $600$ ,  $800$  and  $1000^\circ\text{C}$  sintered samples are given in Table 1. The density decreases from green sample to  $1000^\circ\text{C}$  sintered sample.

Table 2  
Activation energy

Sample	Activation energy (eV)	
	Low temperature	High temperature
$600^\circ\text{C}$	0.57	0.14
$800^\circ\text{C}$	0.22	0.11
$1000^\circ\text{C}$	0.19	0.10

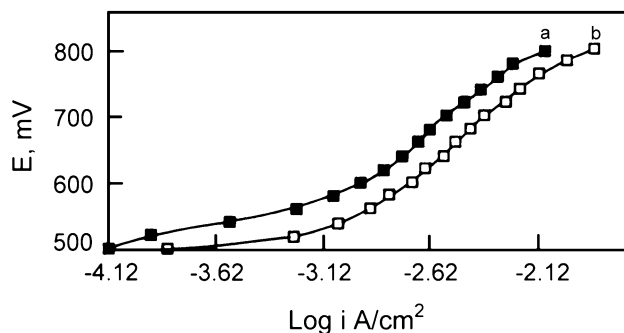


Fig. 6. Tafel plot of (a) 800 °C and (b) 1000 °C sintered samples.

The decrease in density is about 24% from going to the material sintered at highest temperature of 1000 °C. Normally in solid compounds, the density used to get increased during sintering. But in this case it is reverse. This behavior may be the results of breaking of numerous bonds in solid solutions, likewise many new bonds are formed. The newly formed bonds may be longer giving the desired structure. During such compound formation, both cations and anions are diffused from different regions, resulting a non-stoichiometry in the structure.

The porosity values are found to increase with increase in sintering temperature. This is somewhat contrary to the general observations. It is evident from the porosity values that the number of voids or the free space or volumes of voids within the pellets have been considerably increased with the advent of temperature effect. This expansion of the material by sintering may be due to any structural change or by the loss of matter from the interior creating more and more free space. The increase in porosity may be resulted when gaseous entities like oxygen or constituted oxides are lost on heating at higher temperature. The observation once again helps to strengthen the complementary nature of porosity and density, that is to say when the former decreases latter increases or vice versa. More so the above observations support the proximity of both the parameters.

For any material to serve as electrodes, mechanical strength is also an essential property such as hardness. The hardness of green sample was not measured since the mechanical strength often was not enough to withstand the

minimum load to be applied for determination. It could be seen from the table that the strength and stability enhances by the sintering process. Therefore it has to be inferred that the new bonds formed are more directional and strong and binding force is increased during the transformation of mixed solid solutions into a desired new material.

### 3.4. Electrical properties

Fig. 5 shows the relationship between the DC electrical conductivity and temperature of the samples sintered at 600, 800 and 1000 °C. It can be seen that in all cases, the conductivity increases with increase in measuring temperature as well as with sintering temperature but the latter plays a dominant role in the enhancement. These observations clearly indicate that the materials are semiconductors. At lower sintering temperature at 600 °C, the material shows poor conduction may either be due to the absence of required current carriers, insufficient thermal energy to overcome the band gap or the presence of impurities. Increasing sintering temperature increases the rate of phase formation of  $\text{SrFeO}_{3-\delta}$  perovskite, which enhances the number of current carriers and in turn the conduction. The 1000 °C sintered sample gave the maximum conductivity of  $84 \text{ S cm}^{-1}$  measured at 1000 °C. In general, in the non-stoichiometric perovskite-type oxides, the conductivity mainly depends upon the holes, electronic and ionic concentration. The electrical property of the  $\text{SrFeO}_{3-\delta}$  has been elaborately studied by Kozhevnikov et al. [15]. As earlier reported, the  $\text{SrFeO}_{3-\delta}$  is a p-type semiconductor [16]. As the sintering temperature increases, the oxygen ion concentration is increased, i.e. the hole concentration increases thus an increase in ionic conductivity. The conducting mechanism of the synthesized materials can be assigned to the following redox reactions



The activation energies calculated for the samples sintered at 600, 800 and 1000 °C from the Arrhenius

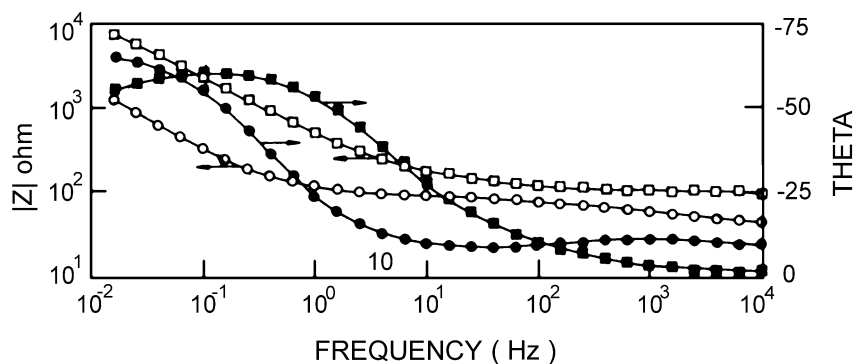


Fig. 7. The typical Bode plot of  $\text{SrFeO}_{3-\delta}$  sintered at 1000 °C (—○—, —●—) and 800 °C (—■—, —□—).

plot are given in Table 2. As can be seen from the table, there are two prominent regions with different slopes corresponding to lower and higher temperatures. As the temperature increases, the activation energy decreases irrespective of the sintering temperature. Likewise with sintering temperature, the values also decrease in both the regions. This indicates an increase in ionic conduction with temperature. Generally, a change in slope is attributed to a change in conducting mechanism, which in turn results to structural changes and transitions [17]. The higher activation energy that resulted at low temperature may be due to the low conduction by electrons between  $\text{Fe}^{2+}$  and  $\text{Fe}^{3+}$ . Contrarily, low activation energy observed at higher temperature is due to different mechanism by hopping of polarons. It has been reported that at lower temperature the  $\text{SrFeO}_{3-\delta}$  possesses tetragonal structure and at higher temperature orthorhombic brownmillerite structure [9]. The difference in activation energy between different sintered specimens is large at low temperature than at higher temperature as evident from the table. This further shows that the effect of temperature is more pronounced at low temperature regions.

### 3.5. Electrochemical properties

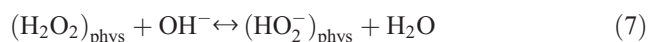
The Tafel plots of  $iR$  free anodic polarization for the synthesized  $\text{SrFeO}_{3-\delta}$  electrodes materials sintered at 800 and 1000 °C in 1 M KOH solutions under potentiostatic conditions are shown in Fig. 6. The Tafel slope for oxygen evolution was calculated from the plots. It is observed that the Tafel slope ( $b_a$ ) is decreased with increasing sintering temperature. At low oxygen overpotential region, the value of 80 mV/dec for 1000 °C sintered sample and 70 mV/dec for 800 °C sintered sample are observed. The change in Tafel slope may be due to a change in conducting mechanism as well as with the intrinsic activity of the cations in the single phase formed in the 1000 °C sintered sample. It can also be seen that the electrocatalytic activity for oxygen evolution reaction increased with increasing sintering temperature. The oxygen overpotential ( $\eta$ ), which decreases with increasing sintering temperature, indicates the decrease of polarization and diffusion overpotential. The overpotential gave 0.462 V for 1000 °C sintered sample and 0.492 V for 800 °C sintered sample at an applied current density 0.8 A/cm<sup>2</sup>. In our study, 1000 °C sintered sample gave oxygen overpotential of 0.4 V at 10 mA/cm<sup>2</sup>. Similar result of 0.38–0.4 V at 10 mA/cm<sup>2</sup> was observed in the earlier study for the  $\text{SrFeO}_{3-\delta}$  sample prepared from solid-state reaction sintered at 1300 °C [18]. The advantage of this co-precipitated sample is that with lower sintering temperature minimum overpotential has been attained.

According to Goodenough [19], the electrons are conducted to the empty  $\sigma^*$  band from the partially filled  $\pi_{\beta}^*$

Table 3  
Impedance parameters

Sample	$C_{dl}$ , mF/cm <sup>2</sup>	$R_f$
800 °C	4.098	68
1000 °C	0.385	6.4

band. Therefore it enhances the oxygen evolution reaction. The reaction mechanism of the oxygen evolution of the synthesized  $\text{SrFeO}_{3-\delta}$  electrode is as follows [20].



where  $\text{M}^z$  is a transition metal ion with a valency state  $z^+$  at the surface of the perovskite.

The complex impedance Bode plots for the co-precipitated  $\text{SrFeO}_{3-\delta}$  at different sintering temperatures 800 and 1000 °C in 1 M KOH solution are shown in Fig. 7. The plots at high and low frequencies are associated with the charge transfer and the mass transfer processes, respectively. The electrochemically active area, i.e. the roughness factor ( $R_f$ ) of the electrocatalyst, was estimated from the ratio of double layer capacitance ( $C_{dl}$ ) of the bulk sample surface/electrolyte interface and the  $C_{dl}$  of the smooth oxide surface (60  $\mu\text{F}/\text{cm}^2$ ). The  $R_f$  and  $C_{dl}$  values of the synthesized samples are given in Table 3. From the table, it is observed that as the sintering temperature increases, the double-layer capacitance decreases as well as the roughness factor. It can be inferred that as the  $C_{dl}$  value decreases, the degradation of the material decreases. Hence the material sintered at 1000 °C is more stable than the sample sintered at 800 °C.

## 4. Conclusion

The Co-precipitation synthesis is found to be a versatile method for preparing new materials. The electrical conductivity measurements have confirmed the semi-conducting nature of the synthesized material with a maximum electrical conductivity of 84 S cm<sup>-1</sup>. On sintering, the stability of the electrode is observed to increase, in spite of an increase in porosity as evidenced from the hardness and  $C_{dl}$  values. The structural studies showed that the synthesized compound possess an orthorhombic structure. From the overall physical, electrical and electrochemical properties, the 1000 °C sintered sample is more suitable for electrode material in metallurgical applications.

## References

- [1] P. Porta, S. Cimino, S.D. Rossi, M. Faticanti, I. Peltiti, *Mater. Chem. Phys.* 71 (2001) 165.
- [2] S.P. Sinmer, J.F. Bonnett, N.L. Canfield, K.D. Meinhardt, J.W. Stevenson, *J. Power Sources* 113 (2003) 1.
- [3] T. Ishihara, Y. Tsuruta, Y. Chunying, T. Todaka, Y. Takita, *J. Electrochem. Soc.* 150 (1) (2003) E17.
- [4] C.O. Augustin, K.S. Srinivasan, *Bull. Electrochem. Soc.* 1 (1985) 56.
- [5] Z. Tianshu, P. Hing, Z. Jiancheng, K. Lingbing, *Mater. Chem. Phys.* 61 (1999) 192.
- [6] P.S. Anil Kumar, J.J. Shrotri, S.D. Kulkarni, C.E. Deshpande, S.K. Date, *Mater. Lett.* 27 (1996) 293.
- [7] C.O. Augustin, D. Prabhakaran, L.K. Srinivasan, *J. Mater. Sci. Lett.* 12 (1993) 383.
- [8] J.P. Singh, N.K. Singh, R.N. Singh, *Int. J. Hydrogen Energy* 24 (1999) 433.
- [9] C. Okazoe, Y. Takeda, N. Imanishi, O. Yamamoto, M. Takano, R. Kanno, *Solid State Ionics* 86–88 (1996) 1431.
- [10] V. Thangadurai, P. Schmid-Beurmann, W. Weppner, *Mater. Res. Bull.* 37 (2002) 599.
- [11] J.T. Last, *Phys. Rev.* 105 (1957) 1740.
- [12] K. Li, F. Wu, D. Wang, T. Xie, T. Li, *Mater. Chem. Phys.* 71 (2001) 34.
- [13] X. Li, H. Zhang, S. Li, W. Fan, M. Zhao, *Mater. Chem. Phys.* 41 (1995) 41.
- [14] R.V. Mangalaraja, S. Ananatha Kumar, F.D. Gnanam, *Mater. Lett.* 57 (2003) 2662.
- [15] V.L. Kozhevnikov, J.A. Leonidov, M.V. Patrokeeve, E.B. Mitberg, K.R. Poeppelmeier, *J. Solid State Chem.* 158 (2000) 320.
- [16] F.W. Poulser, G. Laurstad, R. Tunold, *Solid State Ionics* 72 (1994) 47.
- [17] D. Ravinder, B. Ravikumar, *Mater. Lett.* 57 (2003) 1738.
- [18] Y. Matsumoto, J. Kurimoto, E. Sato, *J. Electroanal. Chem.* 102 (1979) 77.
- [19] J.B. Goodenough, *J. Appl. Phys.* 37 (1966) 1415.
- [20] J.O.M. Bockris, T. Otagawa, *J. Phys. Chem.* 87 (1983) 2960.